



This is a repository copy of *Using the Reynolds stress model to predict shock-induced separation on transport aircraft*.

White Rose Research Online URL for this paper:

<https://eprints.whiterose.ac.uk/135653/>

Version: Accepted Version

Article:

Apetrei, R., Curiel-Sosa, J.L. orcid.org/0000-0003-4437-1439 and Qin, N. (2019) Using the Reynolds stress model to predict shock-induced separation on transport aircraft. *Journal of Aircraft*, 56 (2). ISSN 0021-8669

<https://doi.org/10.2514/1.C034968>

© 2018 by R. M. Apetrei, J. L. Curiel-Sosa, and N. Qin. This is an author produced version of a paper subsequently published in *Journal of Aircraft*. Uploaded in accordance with the publisher's self-archiving policy. Razvan M. Apetrei, Jose L. Curiel-Sosa, and Ning Qin. "Using the Reynolds Stress Model to Predict Shock-Induced Separation on Transport Aircraft", *Journal of Aircraft*, <https://doi.org/10.2514/1.C034968>

Reuse

Items deposited in White Rose Research Online are protected by copyright, with all rights reserved unless indicated otherwise. They may be downloaded and/or printed for private study, or other acts as permitted by national copyright laws. The publisher or other rights holders may allow further reproduction and re-use of the full text version. This is indicated by the licence information on the White Rose Research Online record for the item.

Takedown

If you consider content in White Rose Research Online to be in breach of UK law, please notify us by emailing eprints@whiterose.ac.uk including the URL of the record and the reason for the withdrawal request.



eprints@whiterose.ac.uk
<https://eprints.whiterose.ac.uk/>

Using the Reynolds Stress Turbulence Model to Predict Shock-Induced Separation on the Common Research Model

Razvan M. Apetrei,^{*} Jose L. Curiel-Sosa,[†] and Ning Qin[‡]

The University of Sheffield, Department of Mechanical Engineering, Sheffield, South Yorkshire, S1 3JD, England

Additional results about the wing-body of the NASA Common Research Model at flight conditions derived from those of the AIAA Computational Fluid Dynamics Drag Prediction Workshop are introduced in this paper. An initial assessment compared the widely used Shear Stress Transport model with the full Reynolds Stress Model as two possible closures for the RANS problem. The study, based on the 6th AIAA Computational Fluid Dynamics Drag Prediction Workshop, confirmed the limitations of linear eddy-viscosity turbulence models in highly anisotropic turbulent flows. A larger than previous experiments reported side-of-body separation was predicted by the Shear Stress Transport model. By comparison, the study revealed that the Reynolds Stress Model is capable of simulating higher incidence transonic flight as the trends observed in the results were in overall good agreement with the experiment. The aim herein was to investigate the high-incidence transonic aerodynamics about the Common Research Model. Using RANS closed with the Reynolds Stress Model, the aeroelastically deformed Common Research Model was then simulated at incidences outside of the Drag Prediction Workshop remit. The evolution of shock-induced boundary layer separation is observed. A separation bubble is first predicted at an incidence of 3.5 degrees, then developed in chordwise and spanwise direction, triggering the stall of the aircraft at an incidence of 5.75 degrees. Using shear-lines helps understand the three-dimensionality of this phenomenon as large areas of crossflow are present starting in the wing-kink region and extending towards the wingtip.

Nomenclature

C_D	=	drag coefficient
C_L	=	lift coefficient
C_M	=	pitching moment coefficient
C_P	=	pressure coefficient
c	=	chord, m

^{*} PhD Student, Computer-Aided Aerospace and Mechanical Engineering (CA²M) Research Group

[†] Lecturer in Aircraft Design and Aeroelasticity, head of CA²M Research Group, www.jlcurielsosa.com

[‡] Professor of Aerodynamics, AFAIAA

dc = drag count = 10^{-4}
 M = Mach Number
 N = Number of nodes
 Re = Reynolds Number
 x,y = streamwise and spanwise directions, m
 α = angle of attack, degrees
 η = normalised spanwise location

Subscripts

max = maximum

I. Introduction

THE PRESENCE of strong Shock-Wave Boundary Layer Interactions (SWBLI) in transonic flow was first reported in 1940s [1] when Hilton and Fowler observed an unsteady behavior characterized by shock movement coupled with unsteady boundary layer separation. Eight decades later, the phenomena governing off-design transonic flight are yet to be fully understood. Technological advancement has allowed for the use of high fidelity Computational Fluid Dynamics (CFD) codes to be used alongside wind tunnel testing for design and optimization of modern transport aircraft. The capabilities of accurately predicting design point lift, drag, and pitching moment exist, are mature and have been validated countless of times within the framework of the AIAA CFD Drag Prediction Workshops[§] (DPW). In the summaries of the 4th, 5th, and 6th DPW [2]–[4] and special editions of Journal of Aircraft dedicated to the DPW [5], [6] the majority of the participants were able to obtain satisfactory force and moment predictions at design point of an industry relevant civilian aircraft. Yet, the capability of predicting transonic aerodynamics at off-design flight conditions is still limited. In particular, the DPW organizing committee have repeatedly expressed their concerns with regards to overprediction of side-of-body (SOB) separation which triggered premature stall of the aircraft. In some of the DPW results, the SOB is overpredicted when compared to experimental measurements performed at ONERA [7]. It is widely believed now that this is due to the isotropic modeling of turbulent stresses by the Boussinesq approximation.

[§] <https://aiaa-dpw.larc.nasa.gov/>

Investigation of individually published records of DPW results shows that, compared to linear eddy viscosity models such as Spalart-Allmaras (SA) or the Shear Stress Transport (SST) the full Reynolds Stress Model (RSM) used mainly in [8]–[10] was more reliable with regards to consistency in the results obtained within the last three DPW.

The aim of this paper is to assess the ability to predict off-design transonic aerodynamics by means of RANS coupled with a second-order turbulence closure. Additional results about the NASA CRM aircraft are introduced including some at incidences outside the DPW remit and previous numerical studies. The results are compared with numerical results obtained with a first-order closure, the SST, and experimental data. The structure of this paper is as follows: the geometry and numerical grids are given in Section II, numerical method is described in Section III followed by discussion of the results in Section IV.

II. Geometry and Numerical Grids

The NASA CRM was developed as presented in Ref. [11] in an effort to provide the scientific community with a standardized testbed for CFD validation purposes. Wind tunnel data is easily accessible on the CRM website^{††} and has been published in Refs. [12]–[15].

In this study, the *wing-body* of the *aeroelastically deformed* CRM from the 6th DPW, shown in Figure 1, is used. The deformation of the CRM was intended to match the deformations observed in the wind-tunnel testing (WTT). The development of such geometries is summarized in [16] and similarly validated by means of fluid-structure interaction (FSI) simulations [17]. The CRM closely resembles a modern wide-body aircraft with overall dimensions equal to those given in Table 1.

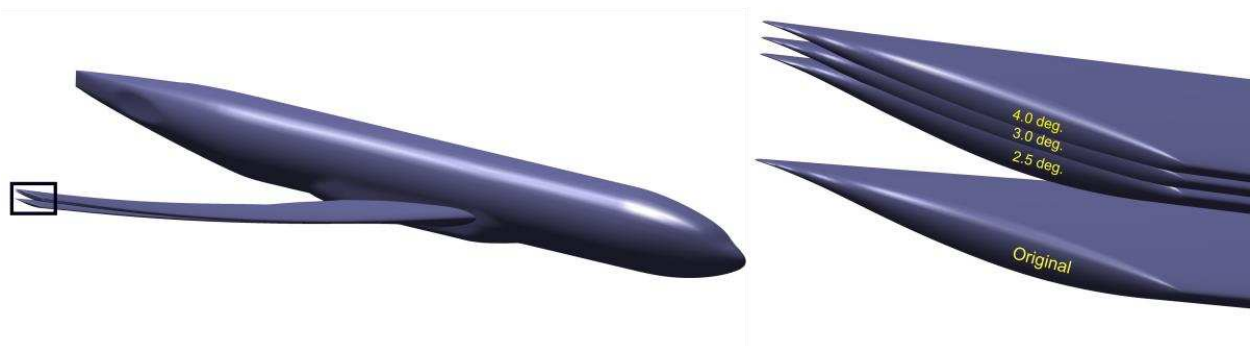


Figure 1. The wing-body CRM: original and deformed due to aerodynamic loading at various incidences.

^{††} <http://commonresearchmodel.larc.nasa.gov/>

A new family of multi-block structured grids was built in ICEM CFD by following the guidelines published by the 6th DPW organizing committee. The aircraft was placed at the center of the symmetry plane on a semi-spherical fluid-domain with a radius of 100 fuselage lengths. There are 181 blocks in total which allowed for the generation of a structured mesh around the complex wing-body geometry. The fuselage and wing were meshed using O-block meshing strategy. Figure 2 shows the blocking distribution around the wing and fuselage. The blocking was initially developed about the undeformed CRM geometry and later adapted to the shapes of the deformed CRM. The grids were modified using translation and / or rotation tools in ICEM CFD while element distribution and sizing was maintained.

Table 1. Geometrical dimensions of the NASA CRM CFD model.

Dimension	CRM
Ref. Area	389.76 m ²
Span	59.226 m
Ref. Chord	7.06 m
Aspect Ratio	9
Taper Ratio	0.275
25% chord Sweep	35.0 degrees

The smallest grid, herein referred to coarse or L3, has just over 11 million nodes. The medium (L2) and fine (L1) were then generated by increasing the number of grid points by a factor of 1.15 in each direction when compared to the previous level. This resulted in about 1.45 increase in total node count from one level to the other. Furthermore, the height of the cell closest to the walls was also reduced by a factor of 1.15 for each level, resulting in a reduced y^+ value. The growth ratio at walls was selected as 1.1. Further details on the grids are given in Table 2. The surface mesh of the finest grid is shown in Figure 3.

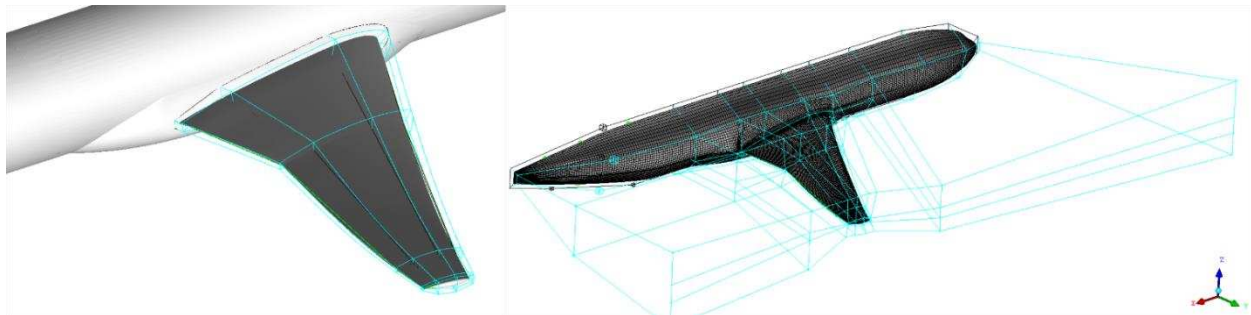


Figure 2. O-grid block structure around the wing (left) and surface mesh with main blocking (right).

Table 2. Details of mesh sizing around the CRM.

Dimension	Mesh
-----------	------

	L3 (coarse)	L2 (medium)	L1 (fine)
Nodes count	11,024,704	16,725,672	25,846,324
First cell height (m)	$3.2 \cdot 10^{-5}$	$2.8 \cdot 10^{-5}$	$2.43 \cdot 10^{-5}$
Corresponding y^+ value	1	0.8	0.67
Wing chordwise number of nodes	63	73	86
Wing spanwise number of nodes	205	241	277
Wing trailing/leading-edge number. of nodes	10	12	14
Fuselage length number of nodes	236	274	320

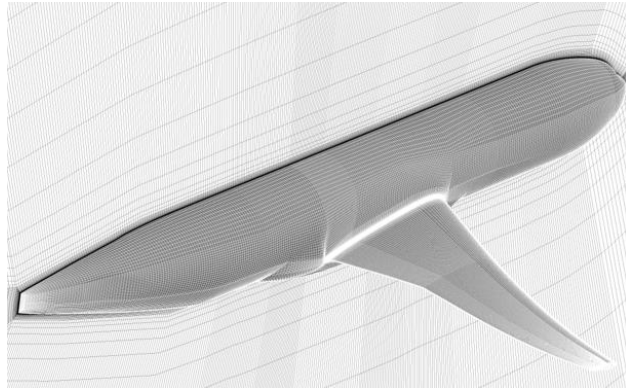


Figure 3. The surface and symmetry plane mesh on L1 grid.

III. Method

The commercial solver ANSYS Fluent was used to solve the RANS equations. The RANS equations were discretized by a second-order upwind scheme; the least squares cell-based method was used for gradients, and then solved using the implicit solver. Two turbulence closures are included in this study. The SST model was chosen to verify the overprediction of the side-of-body separation observed in previous results. The full RSM was then selected as an advanced modelling approach to investigate its potential benefits in prediction of off-design transonic aerodynamics. Compared to the SST model, the RSM does not make use of the Boussinesq approximation and adds 7 equations to the RANS problem: 6 for the Reynolds stresses and one for the dissipation rate. In this study, the Launder-Reece-Rodi) LRR RSM developed in Ref. [18] was used.

The convergence criteria was monitored through the evolution of the global aerodynamic coefficients and the Residuals output in Fluent. An example is visualized in Fig. 4. On the left hand side, the residual decrease for the RSM shows at least 3 orders of magnitude before C_L reached a converged value. A similar observation can be made on the convergence behavior of the SST model. On average, the simulations with SST model converged in 2,500 - 5000 iterations and allowed for convergence acceleration through adaptive Courant Number. In comparison, the RSM

took up to 8 times more iterations before reaching convergence. The RSM was found to be highly sensitive and diverged if Courant Number was too large. Simulations were performed on single grid and the authors appreciate that multigrid methods could have had an impact on convergence speed. All runs were performed on the High Performance Computing (HPC) facilities at The University of Sheffield: Iceberg and ShARC on CPUs ranging from 12 to 96. The computational time, measured in CPU*hours increased tenfold between SST and RSM.

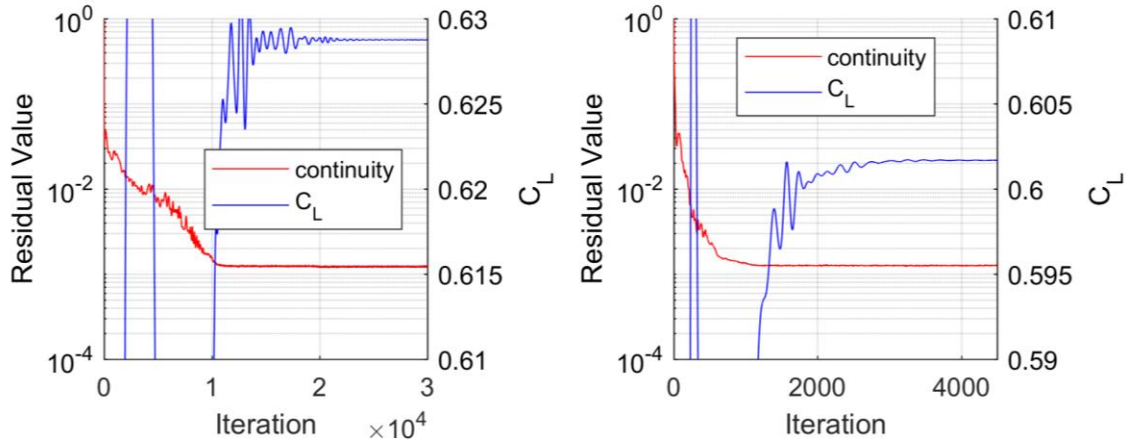


Figure 4. Residual and monitor convergence for RSM (left) and SST (right) at $\alpha = 3.5$ deg.

IV. Results

A complete list of boundary conditions is given in Table 3.

Table 3. Description of boundary conditions for the numerical study.

Mach Number	Reynolds Number	Free stream Temperature, K	Free stream Pressure, Pa	Free stream Turbulence intensity / length scale, m	Alpha, degrees	Geometry Used	Grid	Turbulence Model	
						Which deformation		RSM	SST
0.85	5 million	310	3800	0.5% / 0.49	2.45-2.49	ae 2.75	L1, L2, L3	Y	N
					2.5	ae 2.5	L2	Y	Y
					3	ae 3.0	L2	Y	Y
					3.5	ae 3.5	L2	Y	Y
					4	ae 4.0	L2	Y	Y
					4.5	ae 4.0	L2	Y	N
					5	ae 4.0	L2	Y	N
					5.5	ae 4.0	L2	Y	N
					5.75	ae 4.0	L2	Y	N
				6	ae 4.0	L2	Y	N	

A. Grid-Sensitivity

The grid sensitivity was evaluated at design point $C_L = 0.5$ and aeroelastic deflections at angle of attack 2.75

degrees. The version of Fluent that was used does not have target C_L boundary conditions implemented. Thus, simulations were first run at incidences of 2.2, and 2.75 degrees respectively. The results were used to interpolate and find the incidence at which $C_L = 0.5$ would be achieved. A third simulation was then run at this incidence and the process repeated for all three grids. In each case simulations converged to a C_L value of 0.5 ± 0.0005 . The results are shown in Figs. 5 and 6 in comparison with experimental and the results from AIAA CFD DPW-6. The N value on the horizontal axis represents the number of nodes in the grid and it is given to the power $-2/3$. In Fig. 5 the drag coefficients are shown. The total C_D is overestimated compared to the average result from the DPW-6 by roughly 10 to 15 dc due to overestimation of the viscous drag, $C_{D,V}$. At the time of writing, it was not possible to compare the drag prediction for different elements of the wing-body configuration and whether this drag overprediction is due to fuselage and / or wing drag. Figure 6 shows that C_M and α for $C_L = 0.5$ are within range of the 6th DPW results.

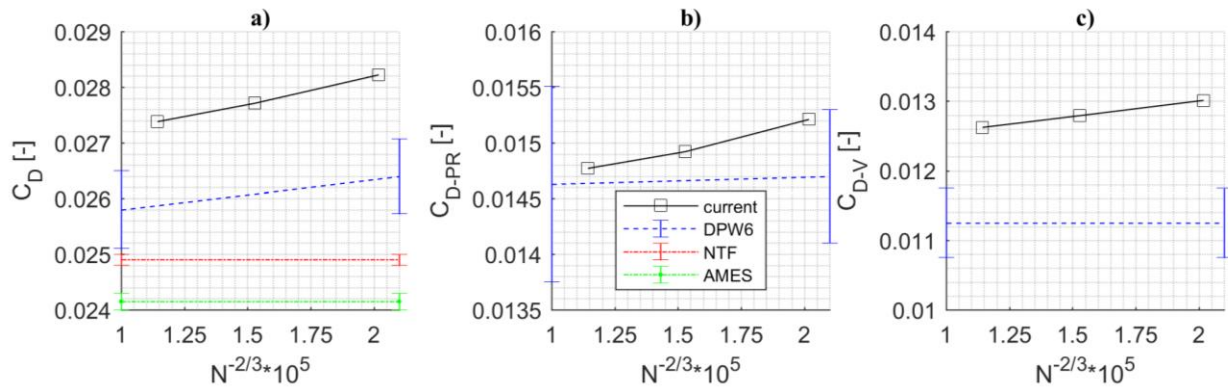


Figure 5. Drag coefficients at different mesh densities: a) total drag, b) pressure drag, and c) viscous drag.

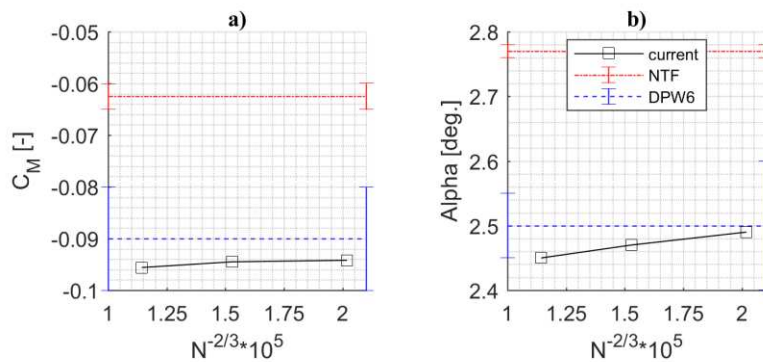


Figure 6. a) Pitching moment coefficient, and b) Angle of attack for $C_L = 0.5$.

More important for this study is the prediction of aerodynamic pressure loads. C_p slices at 6 spanwise locations are given in Fig. 7. The solutions for the three meshes are overall in good agreement. Insignificant differences can be

observed in the strength of the shock at sections closer to wingtip. The CFD results also show good comparison with the experimental data for 5 of the 6 spanwise locations shown. It was found that, the spanwise location $\eta = 0.603$ was designed with high camber and was challenging to predict its pressure recovery even within the 6th DPW [4, 10].

Thus, for the remainder of this study, unless otherwise stated, all the results presented have been obtained with the medium sized grid.

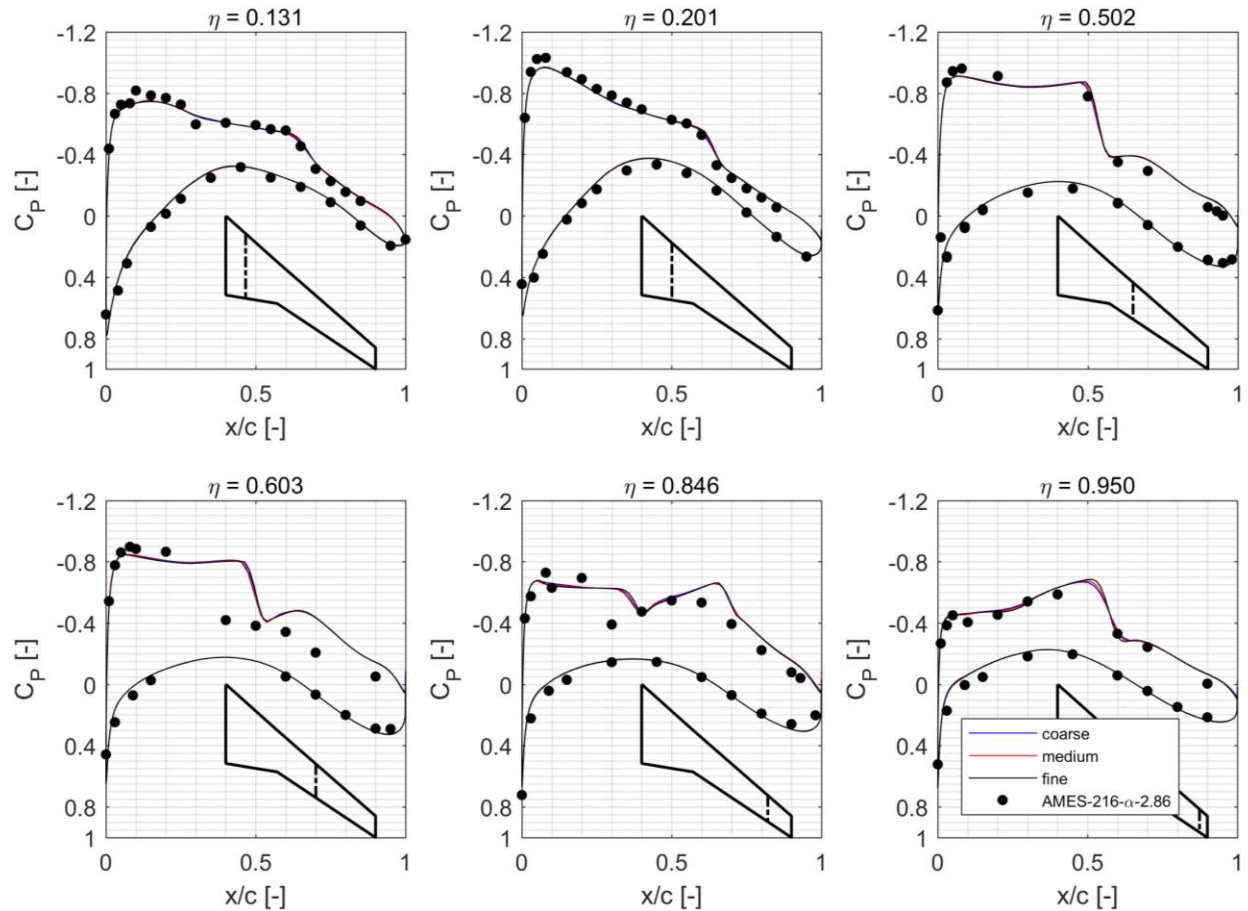


Figure 7. Effect of grid density on C_p .

B. Effect of turbulence modelling

The global C_L , C_D and C_M of the wing-body CRM are presented in Fig. 8 in comparison with experimental data from NTF. At C_L close to the design point of 0.5 the cheaper option of using the SST model produces more accurate results. At off-design flight conditions and higher incidences, the RSM is consistently overpredicting the results but the SST shows a gradual decrease in the $\delta C_L / \delta \alpha$ and ultimately premature stall of the aircraft. As expected, at $\alpha = 4.0$ deg. the SST predicts a large SOB separation producing the stall of the aircraft. In Fig. 9 the SOB is shown through shearlines and isosurfaces of negative streamwise velocity. The C_p contours and shear lines in Fig. 10 indicate that

even before the large SOB separation is present, the SST model predicts a larger shock-induced separation, which can be correlated with the change in $\delta C_L/\delta\alpha$ value. In the C_L vs C_D plot (Fig. 8, b) both turbulence models show an overprediction in drag at design point but results get closer to experiment at higher incidences. The C_M trends captured by RSM are in good agreement with experiment, including the pitch break that occurs after $\alpha = 3.0$ degrees. Similar to previous studies, the C_M is predicted to be more negative, most likely due to lack of corrections applied to wind tunnel data with regards to mounting system effects [4].

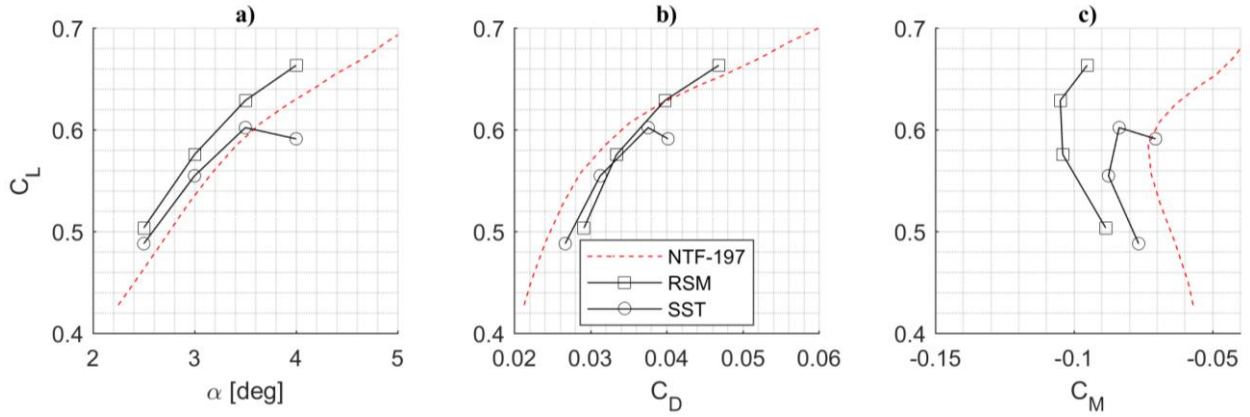


Figure 8. Effect on turbulence model on global aerodynamic coefficients.

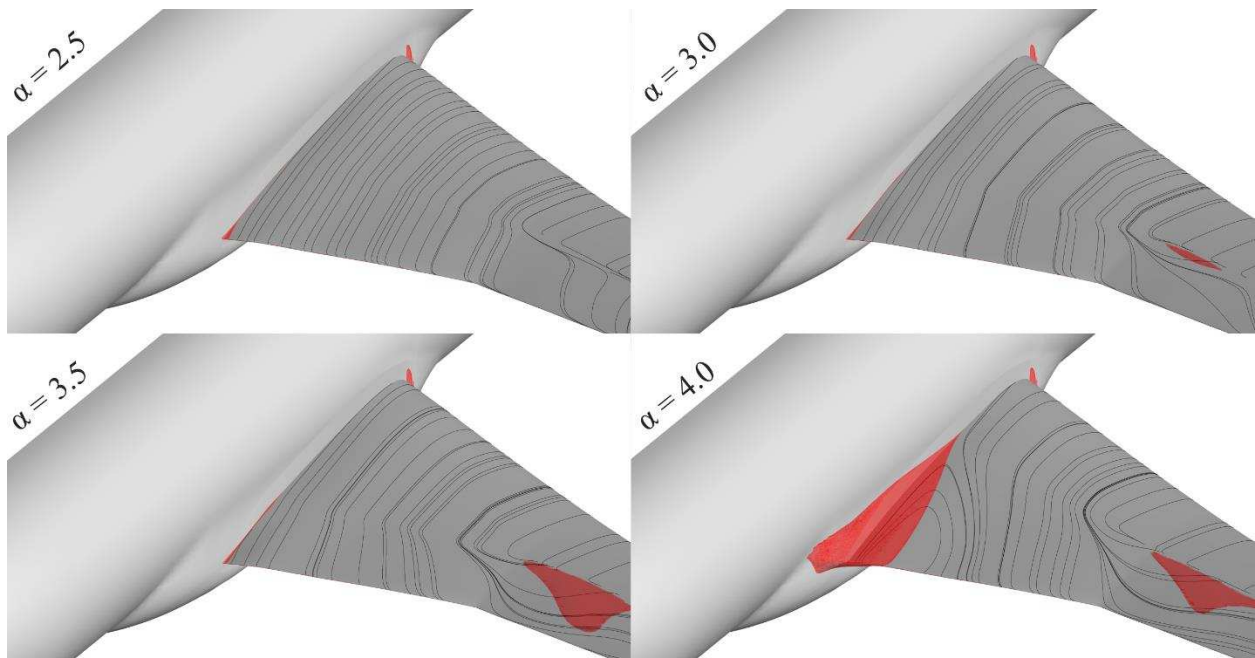


Figure 9. Side-of-body separation observed in the results obtained with the SST turbulence model on the deformed CRM. Isosurfaces of negative streamwise velocity shown in red.

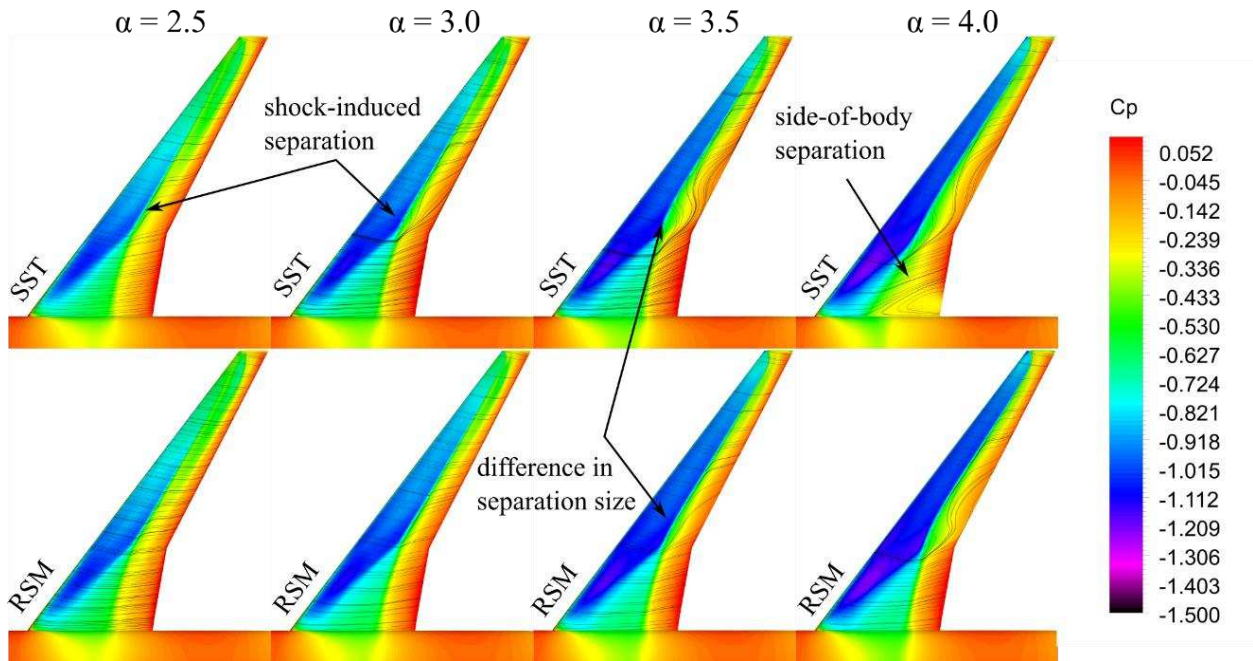


Figure 10. C_p contours on the deformed CRM predicted by SST and RSM .

The comparison between the RSM, SST and experimental C_p at multiple spanwise locations given in Fig. 11 shows the cause of C_L overprediction by the RSM model. Inboard of the wing crank, CFD results are in excellent agreement with experiment, the outer half sections, for η higher than 0.5, show that the shock location is predicted further downstream. The supersonic plateau of C_p is observed to cover a longer portion of the wing resulting in higher loads. The effect of the side-of-body separation is visible for η 0.131 in the SST results at an incidence of 4.0 deg.

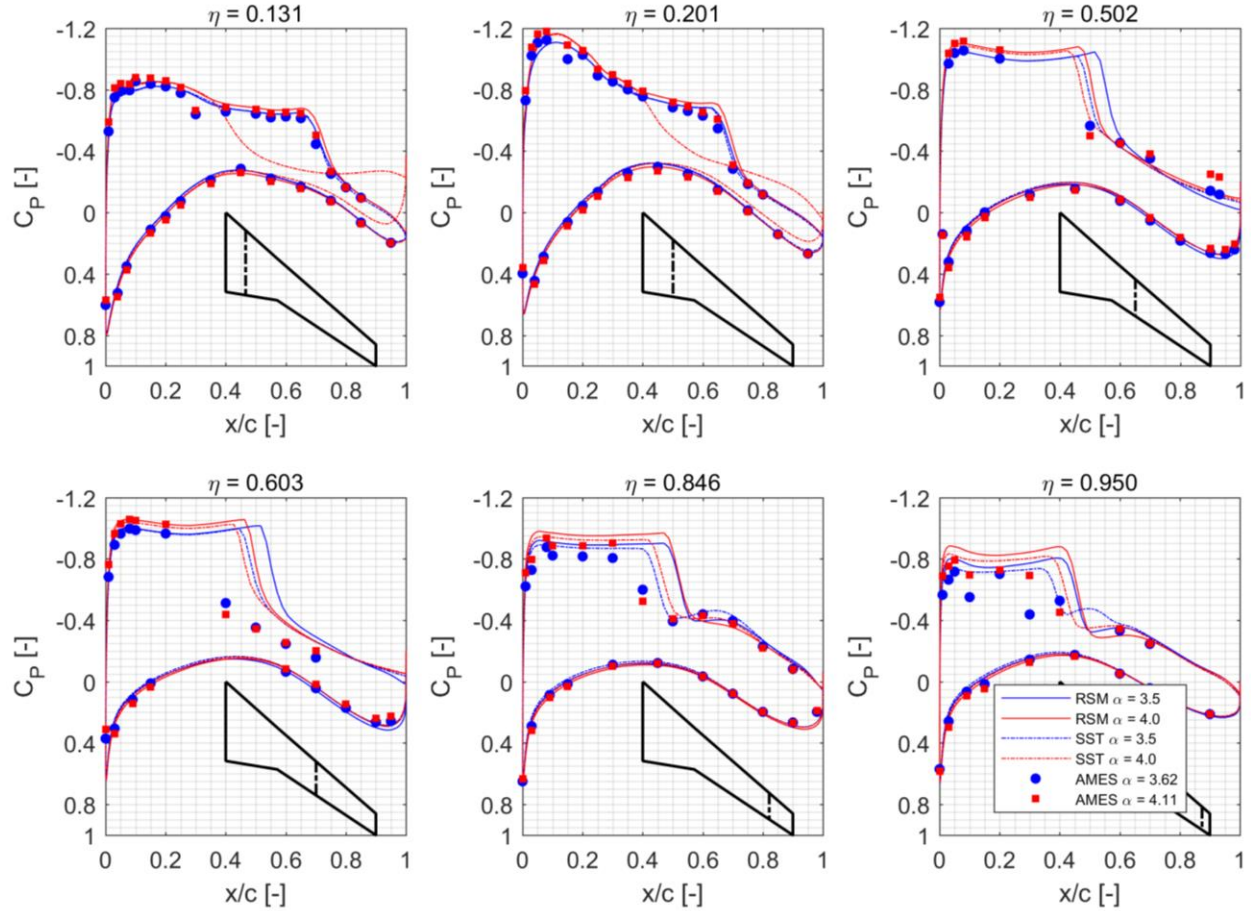


Figure 11. Comparison of C_p distributions between RSM, SST and experimental results.

C. Shock-induced separation at high incidence

The CRM was simulated at higher incidences to evaluate the development of shock-induced boundary layer separation at off-design flight conditions. In the previous section, it was found that the RSM outperformed the SST at higher incidences and that it was a more appropriate choice of turbulence modelling. As such, all the results presented in this section were computed by solving the steady RANS equations closed with the RSM. In this part of the study, the aeroelastically deformed CRM from the 6th DPW, with aeroelastic deformations was used. Simulations were run at incidences higher than 4.0 degrees where the most deformed CRM available (aeroelastic deformations at 4.0 degrees) was used.

The global C_L , C_D and C_M are given in Fig. 12 in comparison with experiment. The $\delta C_L / \delta \alpha$ is in good agreement with experimental data up to an incidence $\alpha = 4.5$ deg. It is followed by a gradual lift break not observed in the experimental data. This is a first indication of increase in the shock-induced separation area [19]. A C_{LMAX} of 0.71 is achieved at $\alpha = 5.75$ deg. followed by a gradual decrease in lift. This value is underpredicted compared to experiment

which shows the stall of the aircraft only much later. Figure 13 gives the shear lines over the top of the wing as the incidence is increased and isosurfaces of negative streamwise velocity. The separation line at the shock foot becomes apparent at $\alpha = 3.0$ deg. followed by a separation bubble at $\alpha = 3.5$ deg. It coincides with a pitch break in Fig. 13. Shock-induced separation is observed to first occur just outboard of the wing-kink. It grows significantly as incidence is increased. By $\alpha = 5.75$ deg., the point of C_{LMAX} , the separation extends to one third of the wing span. The shock-induced separation has little effect on the wing-root aerodynamics, but its three-dimensionality is seen to have an impact on the outboard and wing-tip sections where significant crossflow is present at high incidences. The C_p distributions are given in Fig. 14 for incidences higher than 4 deg. in comparison with experimental data. Shock movement is clearly observed in the mid-wing regions where the shock travel distance can cover up to 25% of local chord.

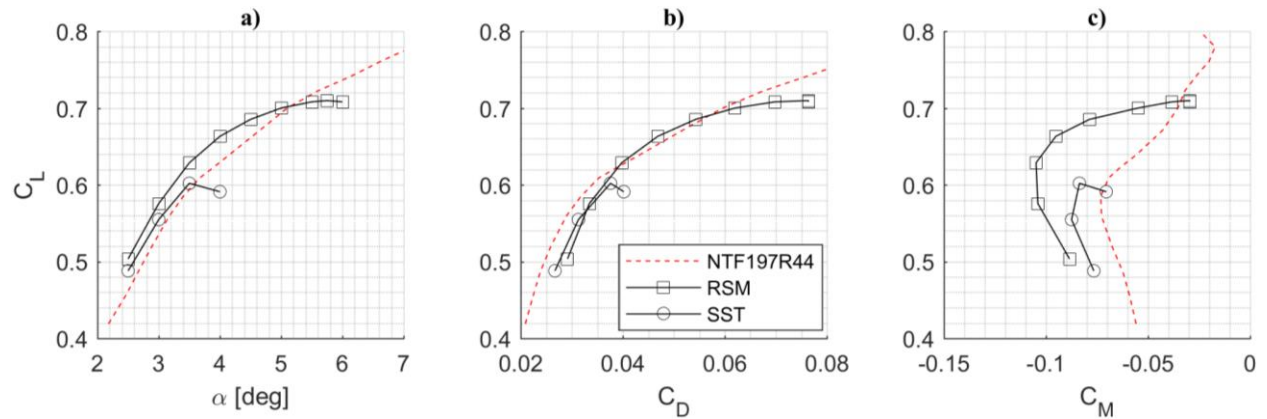


Figure 12. Global aerodynamic coefficients up to stall on the deformed CRM.

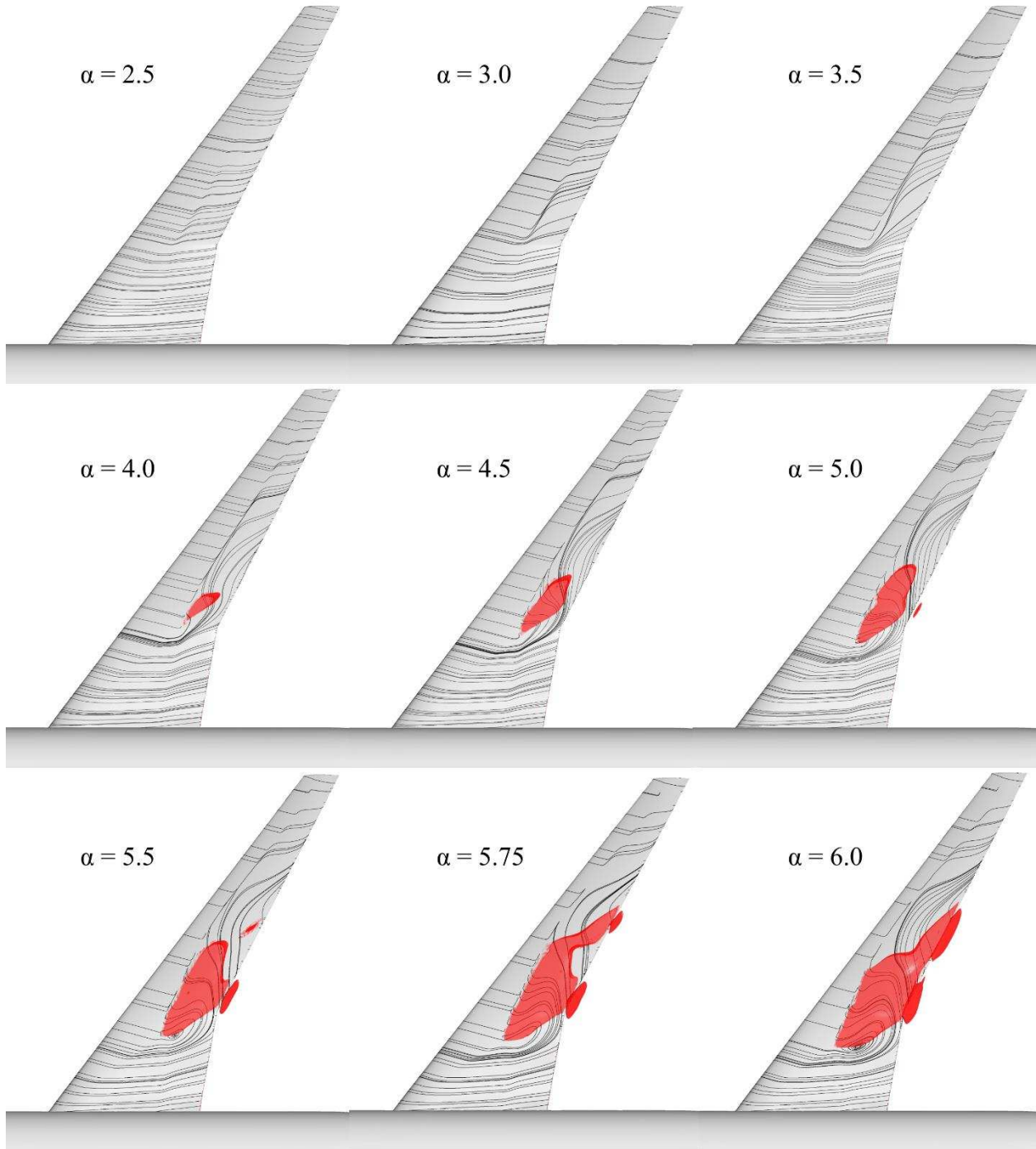


Figure 13. Shear lines and negative streamwise velocity iso-surfaces on the deformed CRM.

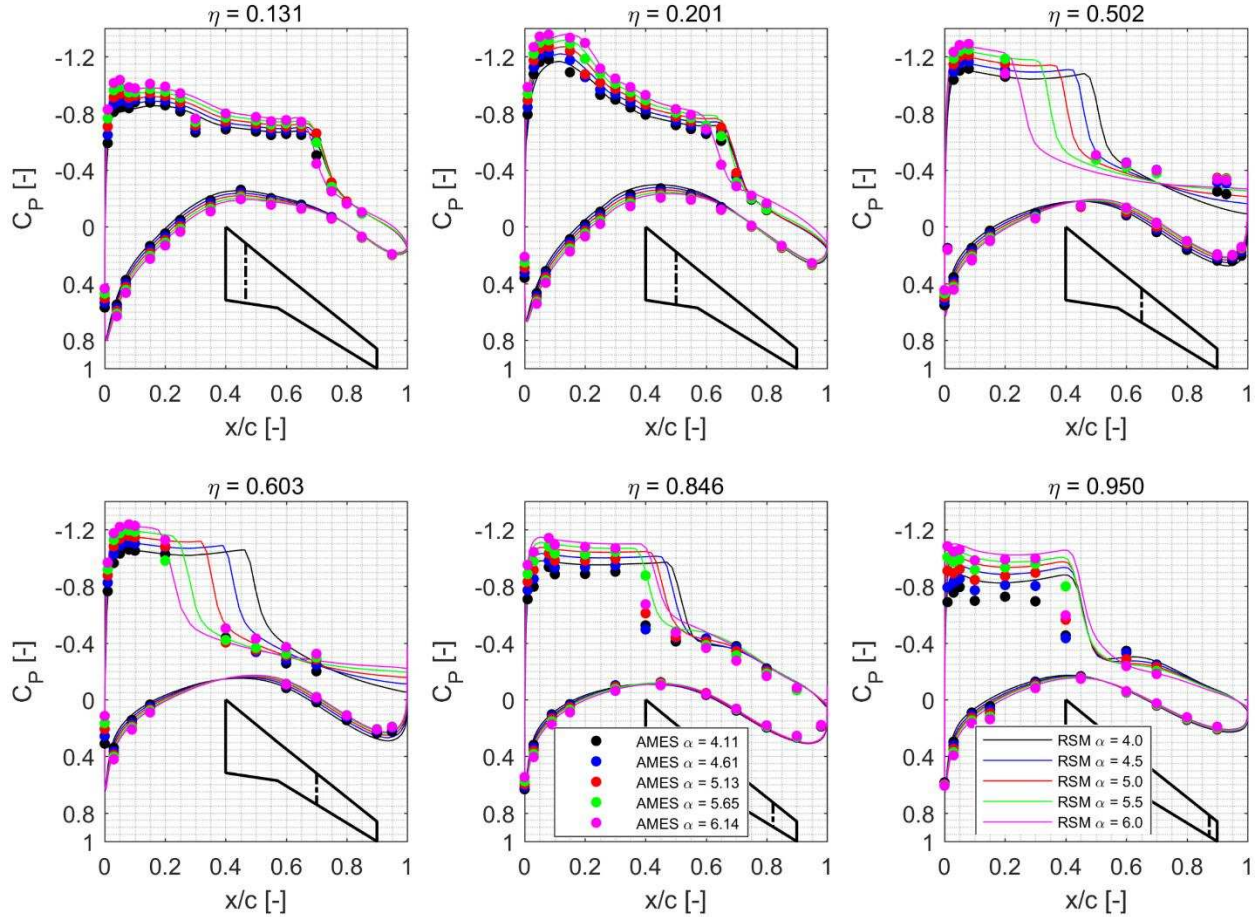


Figure 14. C_p for the deformed CRM at high-incidence. Comparison between CFD and AMES experimental data

V. Conclusions

This paper introduced additional numerical results about the NASA CRM at flight conditions derived from those in the DPW. The aim was to identify any benefits of using the RSM turbulence closure as a substitute to more widely used eddy viscosity models. In an initial validation study, the deformed CRM from DPW-6 was simulated at incidences between 2.5 and 4 deg. using both SST and RSM. The SST model showed considerably better accuracy at design-point incidence but predicted a lift break due to side-of-body separation at higher incidences. In comparison, the RSM consistently overpredicted the C_L as the $\delta C_L / \delta \alpha$ remained in good agreement with that of the experiment. It's worth noting that in exchange for better capture of the high-incidence aerodynamics, the current implementation of RSM inflicted 8 times more computational costs when compared to the SST model. This is primarily due to increased number of iterations required by the RSM model to converge.

In addition, the CRM was also simulated at incidences outside the DPW remit to investigate the prediction of shock-induced separation in off-design transonic flight using the RANS approach closed with the full RSM. As the incidence was increased past 4.0 degrees, the computational results showed a decrease in $\delta C_L/\delta\alpha$ coupled with presence of shock-induced separation. The trends in C_L were not in the same agreement as before with the C_{LMAX} being achieved at an incidence of 5.75 deg. which is lower than what experiments have previously shown. The shear lines on the upper surface indicate propagation of the shock-induced separation to occur in both chordwise and spanwise direction. Specifically, crossflow was present towards the wingtip.

Data

The blocking structure for the mesh, Fluent case setup and data associated with this paper are available after publication through The University of Sheffield ORDA system at: 10.15131/shef.data.5783001

Funding

The authors would like to acknowledge the financial support provided by the University of Sheffield for a PhD studentship that allowed for this study to be completed.

References

[1] F. W. Hilton and R. G. Fowler, "Photographs of Shock Wave Movement," National Physics Laboratory R&M 2692, 1947.

[2] J. C. Vassberg et al, "Summary of the Fourth AIAA CFD Drag Prediction Workshop," Journal of Aircraft, Vol. 51, No. 4 (2014), pp. 1070-1089

[doi: 10.2514/1.C032418](https://doi.org/10.2514/1.C032418)

[3] D. W. Levy et al., "Summary of Data from the Fifth Computational Fluid Dynamics Drag Prediction Workshop," Journal of Aircraft, Vol. 51, No. 4, 2014, pp. 1194–1213.

doi: 10.2514/1.C032389

[4] E. Tinoco et al., "Summary of Data from the Sixth AIAA CFD Drag Prediction Workshop: CRM Cases 2 to 5," 55th AIAA Aerospace Sciences Meeting, Vol. 1, AIAA Grapevine, Texas, 2017.

doi: 10.2514/6.2017-1208

[5] J. C. Vassberg, and E. M. Lee-Rausch, "Drag Prediction Workshop," Journal of Aircraft, Vol. 51, No. 4, 2014 pp. 1069-1331.

[6] J. C. Vassberg, and E. M. Lee-Rausch, "Special Section on Sixth AIAA CFD Drag Prediction Workshop," Journal of Aircraft, Vol. 55, No. 4, 2018 pp. 1317-1509.

[7] A. Cartieri, D. Hue, Q. Chanzy, and O. Atinault, "Experimental Investigations on the Common Research Model at ONERA-S1MA – Comparison with DPW Numerical Results," 55th AIAA Aerospace Sciences Meeting, Vol.1, AIAA Grapevine, Texas, 2017.

doi: [10.2514/6.2017-0964](https://doi.org/10.2514/6.2017-0964)

[8] V. Togiti, B. Eisfeld, and O. Brodersen, "Turbulence model study for the flow around the NASA Common Research Model," *Journal of Aircraft*, Vol. 51, No. 4, 2014, pp. 1331–1343.

doi: 10.2514/1.C032609

[9] O. P. Brodersen, S. Crippa, B. Eisfeld, S. Keye, and S. Geisbauer, "DLR Results from the Fourth AIAA Computational Fluid Dynamics Drag Prediction Workshop," *Journal of Aircraft*, Vol. 51, No. 4, 2014, pp. 1135-1148.

doi: [10.2514/1.C031533](https://doi.org/10.2514/1.C031533)

[10] S. Keye, V. K. Togiti, and O. P. Brodersen, "DLR Results of the Sixth AIAA Computational Fluid Dynamics Drag Prediction Workshop," 35th AIAA Applied Aerodynamics Conference, AIAA AVIATION Forum, Denver, Colorado, 2017.

doi: [10.2514/6.2017-4232](https://doi.org/10.2514/6.2017-4232)

[11] J. Vassberg, M. Dehaan, M. Rivers, and R. Wahls, "Development of a Common Research Model for Applied CFD Validation Studies," 26th AIAA Applied Aerodynamics Conference, Vol. 1, AIAA, Honolulu, Hawaii, 2008.

doi: 10.2514/6.2008-6919

[12] J. Bell, "Pressure-Sensitive Paint Measurements on the NASA Common Research Model in the NASA 11-ft Transonic Wind Tunnel," 49th AIAA Aerospace Sciences Meeting, Vol. 1, AIAA, Orlando, Florida, 2016.

doi: 10.2514/6.2011-1128

[13] M. B. Rivers, and A. Dittberner, "Experimental Investigations of the NASA Common Research Model," *Journal of Aircraft*, Vol. 51, No. 4, 2014, pp. 1183-1193.

doi: [10.2514/1.C032626](https://doi.org/10.2514/1.C032626)

[14] M. B. Rivers, R. Rudnik, and J. Quest, "Comparison of the NASA Common Research Model European Transonic Wind Tunnel Test Data to NASA Test Data," *CEAS Aeronautical Journal*, 2017, pp. 1–11.

doi: 10.1007/s13272-017-0250-7

[15] M. Ueno, M. Kohzai, S. Koga, H. Kato, K. Nakakita, and N. Sudani, "80% Scaled NASA Common Research Model Wind Tunnel Test of JAXA at Relatively Low Reynolds Number," 51st AIAA Aerospace Sciences Meeting, Vol. 1, AIAA, Grapevine, Texas, 2013.

doi: 10.2514/6.2013-493

[16] S. Keye, and M. Gammon, "Development of Deformed CAD Geometries of NASA's Common Research Model for the Sixth AIAA CFD Drag Prediction Workshop," *Journal of Aircraft*, Vol. 55, No. 4, 2018, pp. 1401-1405.

doi: [10.2514/1.C034428](https://doi.org/10.2514/1.C034428)

[17] S. Keye and O. Brodersen, "Investigation of Aero-Elastic Effects on the NASA Common Research Model," *Journal of Aircraft*, Vol. 51, No. 24, 2014, pp. 1323-1330.

doi: 10.2514/1.C032598

[18] B. Launder, G. Reece, and W. Rodi, "Progress in the Development of a Reynolds Stress Turbulence Closure," *Journal of Fluid Mechanics*, Vol. 68, 1975, pp. 537-566.

doi: [10.1017/S0022112075001814](https://doi.org/10.1017/S0022112075001814)

[19] S. Lawson, D. Greenwell, and M. K. Quinn, "Characterisation of Buffet on a Civil Aircraft Wing," 54th AIAA Aerospace Sciences Meeting, Vol. 1, AIAA, San Diego, California, 2016, pp. 1-19.

doi: 10.2514/6.2016-1309